Journal of Electron Spectroscopy and Related Phenomena 181 (2010) 88–95

Contents lists available at ScienceDirect

Journal of Electron Spectroscopy and Related Phenomena

journal homepage: www.elsevier.com/locate/elspec

# Tuning the giant Rashba effect on a $BiAg_2$ surface alloy: Two different approaches

E. Frantzeskakis[a,*], A. Crepaldi[a], S. Pons[a,c], K. Kern[a,b], M. Grioni[a]

[a] Laboratoire de Spectroscopie Électronique, Institut de Physique de la Matière Condensée, École Polytechnique Fédérale de Lausanne (EPFL), Station 3, CH-1015 Lausanne, Switzerland
[b] Max-Planck-Institut für Festkörperforschung, D-70569 Stuttgart, Germany
[c] Département Physique de la Matière et des Materiaux, Institut Jean Lamour, CNRS, Nancy Université, F-5406 Vandoeuvre-les-Nancy, France

ARTICLE INFO

*Article history:*
Available online 4 June 2010

*Keywords:*
Angle-resolved photoelectron spectroscopy
Rashba splitting
Surface states
Quantum-well states
Electron doping

ABSTRACT

We discuss two different approaches for tuning the giant spin–orbit splitting of a $BiAg_2$ surface alloy. The first approach consists of electron doping by alkaline metal deposition in order to shift the energy position of the spin-split surface states, while the second is based on the novel Si(1 1 1)–Ag–$BiAg_2$ trilayer system. In both cases the spin-polarized structure near the Fermi level can be controlled by an external parameter, while the second approach permits coupling the concept of giant spin-splitting with a semiconducting substrate.



## 1. Introduction

The spin degeneracy of electronic states is a consequence of both time reversal and inversion symmetry. The latter is, however, broken for two-dimensional electron gases at surfaces and interfaces. The degeneracy can be then lifted by the effect of the spin–orbit (SO) interaction which results in a modified dispersion of the surface states [1]. This so-called Rashba–Bychkov (RB) effect is the surface analog of the Dresselhaus effect observed in bulk materials which lack an inversion center [2]. An additional term in the otherwise spin-independent Hamiltonian operator captures the coupling of the electron's spin to the magnetic field which appears in the rest frame of the electron. This relativistic Hamiltonian term splits the free-electron parabola into two branches with dispersion:

$$E^{\pm}(k_{//}) = \frac{\hbar^2 k_{//}^2}{2m^*} \pm \alpha_R k_{//} \quad (1)$$

$\alpha_R$, known as the Rashba parameter, is proportional to the out-of-plane surface potential gradient and can be used as a measure of the RB effect magnitude. SO split states were first directly observed by angle-resolved photoemission (ARPES) on the Au(1 1 1) surface [3]. Experimentally, the splitting of the Au(1 1 1) Shockley surface state was found to be several orders of magnitude larger than estimates based on equation (1). This is due to the limitations of the simple free-electron approach which ignores the effect of the strong potential gradient near the ion cores. A more realistic tight-binding model revealed that the size of the splitting depends on the combined effect of the surface potential gradient and the atomic SO coupling [4]. ARPES is an excellent tool for surface states investigation [5] and, up to this date, several metal surfaces which exhibit the RB effect have been studied, confirming qualitatively the theoretical predictions [6–9].

Quantitative discrepancies with the predictions of (1) are surprisingly large for a well-ordered $BiAg_2$ surface alloy, which was found to exhibit a very large Rashba parameter [10]. Based on the results of relativistic first-principle calculations, an additional in-plane potential gradient has been proposed, which can enhance the RB effect [10]. A nearly free-electron (NFE) model generalized the above conclusions for any anisotropic two-dimensional electron gas (2DEG) subject to the SO interaction [11]. An independent theoretical study proposed that the large enhancement can be explained by the distortion of the surface state wavefunction due to the outward buckling of Bi atoms [12]. Similar metallic surface alloys might prove very promising candidates for spintronics applications since they could decrease the spin precession time in a spin transistor and allow distinguishing between the intrinsic and extrinsic Hall effects [13]. One of the main challenges is to control the magnitude and direction of the spin polarization near the Fermi level. This would be possible if one could tune the RB effect at will.

Our research group has demonstrated that a controlled change of stoichiometry in the $Bi_xPb_{1-x}$/Ag(1 1 1) surface alloy permits to control the SO parameters [14]. Although, a continuous tuning of the surface state position is achieved, the main disadvantage of

* Corresponding author. Tel.: +41 021 693 4404; fax: +41 021 693 3604.
*E-mail address:* emmanouil.frantzeskakis@epfl.ch (E. Frantzeskakis).

0368-2048/$ – see front matter © 2010 Elsevier B.V. All rights reserved.
doi:10.1016/j.elspec.2010.05.018

this approach is that the structural disorder of the mixed alloy is reflected into the electronic structure. It should be, however, noted, that the spin structure is not changed by the disorder in the mixed alloy system, as has been shown by Meier et al. [15]. In the present paper we explore two alternative ways to custom tailor the spin-dependent electronic structure of the $BiAg_2$ alloy. The first approach is by means of electron doping along the lines of a similar recent study on the $BiCu_2$ surface alloy [16]. For the second approach, we present new experimental data on the novel Si(1 1 1)–Ag–$BiAg_2$ tri-layer system where the buffer layer thickness is the crucial external parameter.

## 2. Experimental details

The samples were prepared in ultra high vacuum using a multichamber setup with a base pressure of $1 \times 10^{-10}$ mbar. The Ag(1 1 1) surface was cleaned by successive cycles of sputtering and annealing at 800 K. During the last part of the annealing the temperature was reduced to 500 K, and 1/3 ML of Bi was deposited on a warm substrate. This procedure produces better surface ordering with respect to the one with Bi deposition at room temperature (RT) followed by a mild annealing at 500 K. The structural quality of the $BiAg_2$–Ag(1 1 1) surface alloy was verified by means of low energy electron diffraction (LEED) which showed a homogeneous $\sqrt{3} \times \sqrt{3}R30^\circ$ reconstruction. The alkali metal (Na) deposition was performed using commercial thermal evaporation dispensers from SAES Getters. The dispensers were previously outgassed and evaporation was achieved with a current equal to 6.5 A. Na evaporation was done on a cold sample (100 K) and the exposure time was limited to 30 s in order to avoid heating the interface.

The Si(1 1 1) substrate (n-type, $\rho = 0.009$–$0.011\ \Omega$ cm) was cleaned by repeated flashes at 1400 K using direct current injection. After the surface was slowly cooled to RT, a sharp $7 \times 7$ LEED signature revealed its atomic order. Ag was deposited by a home-made Knudsen cell while the sample was kept at 80 K. The Ag thin film grows in the [1 1 1] direction and LEED reveals a $1 \times 1$ symmetry similar to that of the clean Ag(1 1 1) surface. After the deposition of 1/3 ML of Bi followed by a mild annealing, the LEED pattern changed to $\sqrt{3} \times \sqrt{3}R30^\circ$ which is the signature of the $BiAg_2$ alloy formation.

ARPES experiments were carried out at RT and 70 K using a Phoibos 150 SPECS Analyzer with an energy resolution better than 5 meV. The base pressure was in the low $10^{-10}$ mbar range. The sample was illuminated with a monochromatized and partially polarized UV light of 21.2 eV from a Gammadata source. During the measurement the pressure in the ARPES chamber was equal to $5 \times 10^{-9}$ mbar (mainly He gas). The wide acceptance angle ($\pm 12^\circ$) of the spectrometer allowed a large part of the surface Brillouin zone (SBZ) to be covered within a single measurement.

## 3. Results

### 3.1. $BiAg_2$–Ag(1 1 1)

A schematic representation of the $BiAg_2$–Ag(1 1 1) surface alloy structure is depicted in Fig. 1a. Each Bi atom is surrounded by six Ag atoms giving rise to a $\sqrt{3} \times \sqrt{3}R30^\circ$ periodicity. The latter is reflected in the SBZ of the system (Fig. 1b), where the primed letters represent the high-symmetry points of the reconstruction.

Fig. 2a follows the surface state dispersion of the $BiAg_2$ alloy along the $\overline{\Gamma M}$ direction of the reconstruction (i.e. $\overline{\Gamma M'}$): in good agreement with previous studies [10,17], it is possible to observe the crossing of two alloy-derived spin-split states of an $sp_z$ character at a binding energy ($E_B$) of 350 meV. Another pair of weaker spin-split bands is pointed out by arrows. The latter have

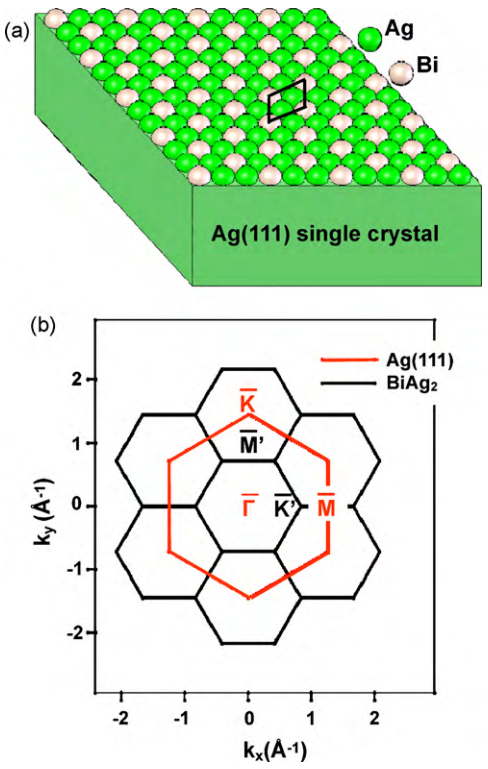


**Fig. 1.** (a) A schematic illustration of the $BiAg_2$–Ag(1 1 1) structure. (b) Surface Brillouin zones of the $BiAg_2$ surface alloy (black) and the substrate (red). Primed (unprimed) letters refer to the high-symmetry points of the reconstruction (substrate). (For interpretation of the references to color in this figure legend, the reader is referred to the web version of the article.)

mainly a $p_{xy}$ character [10,12] and cross the Fermi level with $k_{F1} = \pm 0.095$ Å$^{-1}$ for the internal branches and $k_{F2} = \pm 0.29$ Å$^{-1}$ for the external ones.

Fig. 2b–f shows the modified surface state dispersion after each successive Na evaporation. Each evaporation time was fixed at 30 s and the measurement was performed when the sample attained a temperature of 70 K. The total amount of Na is continuously increasing from Fig. 2b to Fig. 2f. After the first Na evaporation, the whole band structure shifts to higher $E_B$: the $sp_z$ crossing shifts by 45 meV and the $p_{xy}$ states straddle the Fermi level at $k_{F1} = \pm 0.08$ Å$^{-1}$ and $k_{F2} = 0.275$ Å$^{-1}$.

After each successive Na deposition, one can observe a continuous and uniform energy shift of all the surface-derived bands, while $k_{F1}$ and $k_{F2}$ continue approaching each other. By fitting the spin-split branches using successive momentum distribution curves, we obtained a total energy shift of about 230 meV after five evaporation cycles. This corresponds to saturation coverage, since further Na deposition does not shift the bands but only increases the structural disorder. The latter is reflected in the visibility of the bands which is strongly diminished. In analogy with a similar study of the Na-doped $BiCu_2$ alloy, saturation is achieved for 0.25 ML of Na [16]. Using this value as a reference, we can conclude that each successive evaporation cycle adds 0.05 ML of Na to our system.

We modelled the experimental results of Fig. 2 by using a simple model which takes into account the RB effect and the momentum distribution anisotropy induced by the in-plane asymmetry of the potential [11]. Working in the momentum representation and considering one electron state from each $p_{xy}$ and $sp_z$ manifolds our basis vectors are $|sp_z\uparrow\rangle$, $|sp_z\downarrow\rangle$, $|p_{xy}\downarrow\rangle$ and $|p_{xy}\uparrow\rangle$. The resulting $4 \times 4$ Hamiltonian matrix consists of two $2 \times 2$ $H_{SO}$ building blocks (one for $sp_z$ and one for $p_{xy}$ bands) and off-diagonal hybridization elements. A group theoretical analysis shows that the real wave-

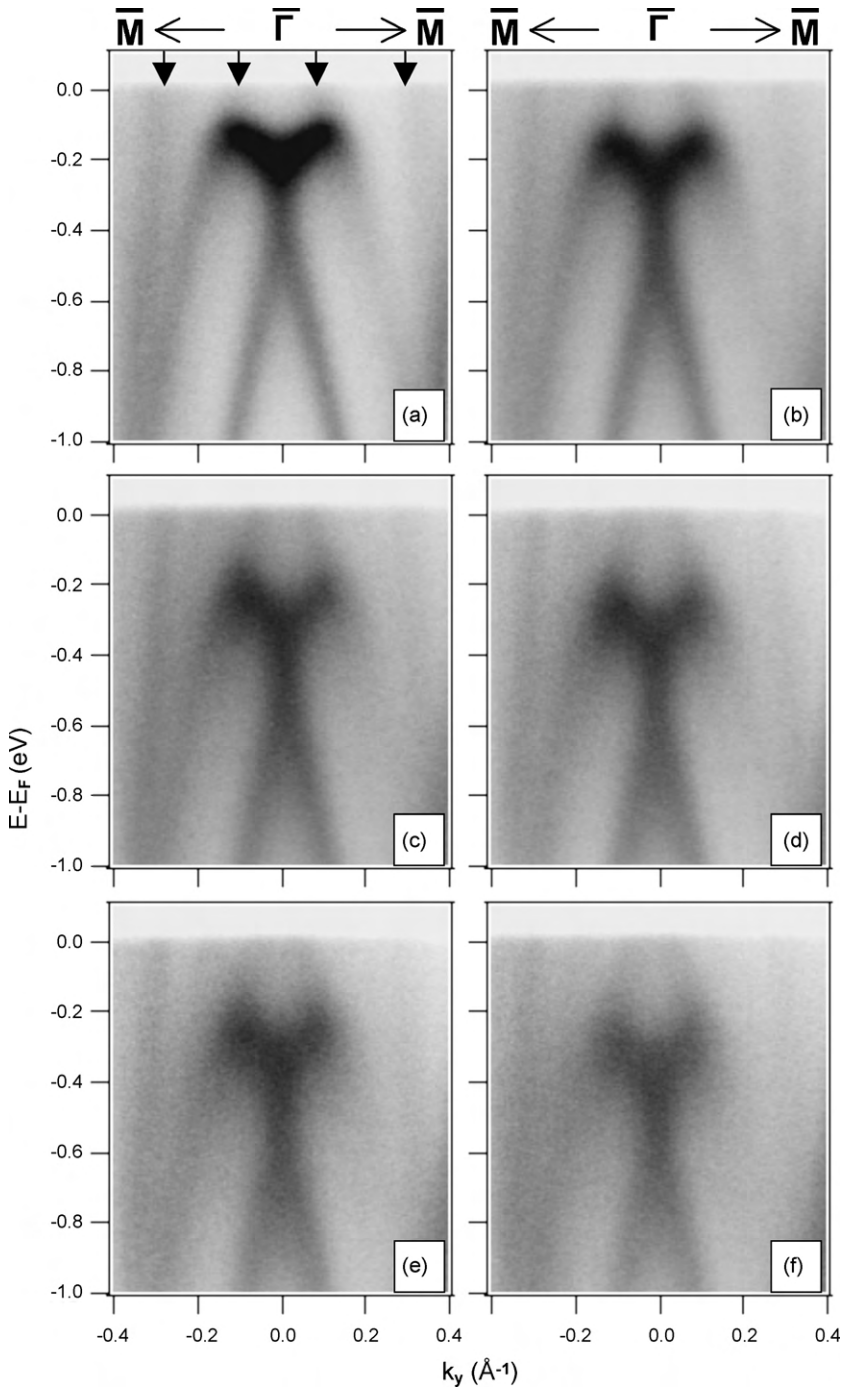


**Fig. 2.** ARPES intensity (70 K) around $\bar{\Gamma}$ for a pure $BiAg_2$–Ag(1 1 1) surface alloy (a) and after electron doping with increasing Na coverage (b–f) (coverage increases from b to f). There is a rigid shift of the whole bandstructure to higher binding energies making the formerly unoccupied states experimentally accessible. The arrows point out the $k_F$ values of the weak $p_{xy}$ spin-split branches.

functions should be represented as appropriate $k$-dependent linear combinations of the above states [18]. Notice also that, due to the SO interaction, spin is not a good quantum number. As a result the outer $sp_z$ band can hybridize with the inner $p_{xy}$ state since they belong to the same representation. This consequence has been taken into account in the structure of our Hamiltonian matrix.

In order to consider the in-plane anisotropy of the potential we used the Hamiltonian proposed by Fu [19]. This is the conventional RB Hamiltonian for a 2DEG with a third-order correction term. The resulting constant-energy (CE) contours (Fig. 3g) are in full agreement with the predictions of an anisotropic 2DEG model with RB splitting [11]. Keeping in mind that each $H_{SO}$ term is given by the sum of the free-electron and the modified Rashba Hamiltonians (i.e. $H_{SO} = H_0 + H_R$) and that the matrix elements of the $2 \times 2$ hybridization blocks ($V_{SS}$) refer to the hybridization potentials between states of a mixed character, the Hamiltonian matrix can be written in this compact form:

$$\begin{pmatrix} H_{SO}(sp_z) & V_{SS} \\ V_{SS}^{*} & H_{SO}(p_{xy}) \end{pmatrix}$$

Fig. 3 summarizes the resulting energy dispersion determined by diagonalizing this matrix. Parameters were chosen to fit the suc-

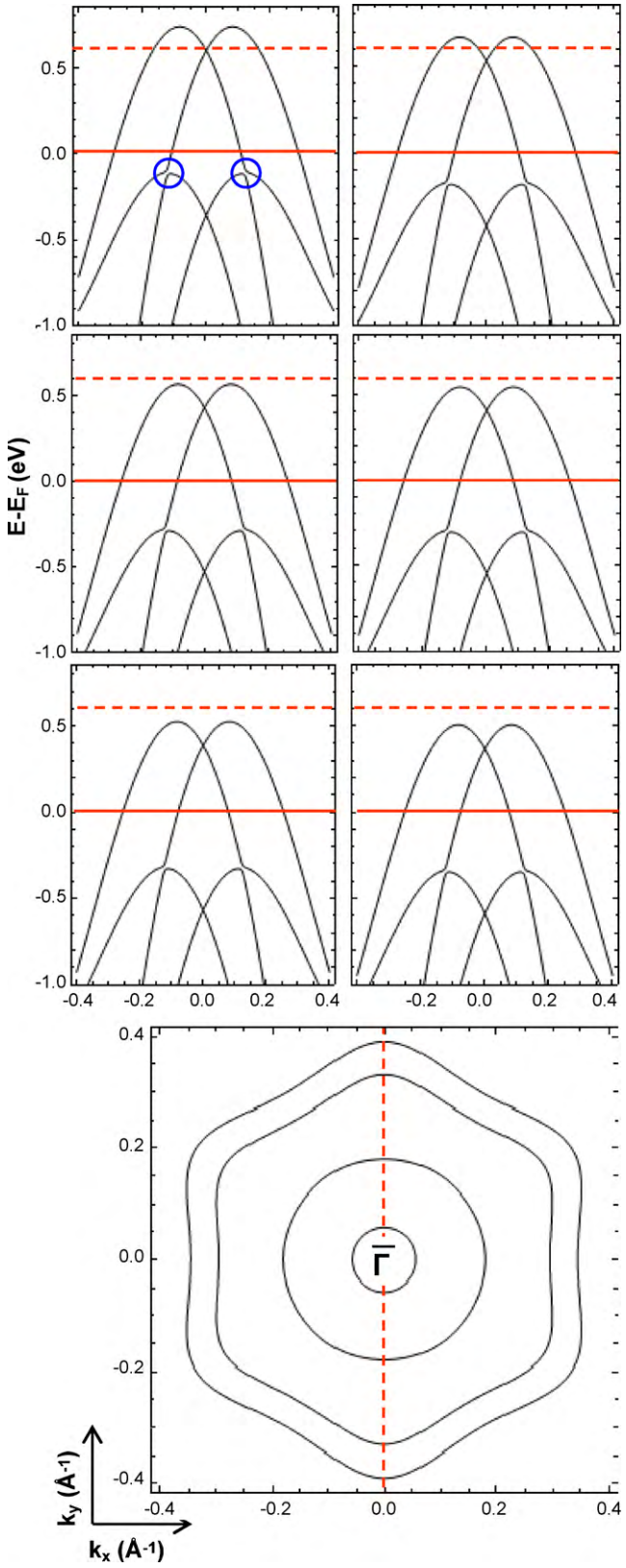


**Fig. 3.** Surface state dispersion around $\bar{\Gamma}$ according to a simple hybridization model: (a) pure $BiAg_2$–Ag(1 1 1) surface alloy, (b–f) $BiAg_2$–Ag(1 1 1) surface alloy with increasing Na coverage in correspondence with the experimental results of Fig. 2. (g) Represents the calculated constant-energy contours for a binding energy of 650 meV. The anisotropic momentum distributions are well reproduced by the model. The horizontal full line shows the Fermi level position, while the horizontal dashed line corresponds to the $p_{xy}$ spin degeneracy point for the pure alloy. The circles point out the hybridization of the surface states. The vertical dashed line follows the direction of the calculated band dispersions.

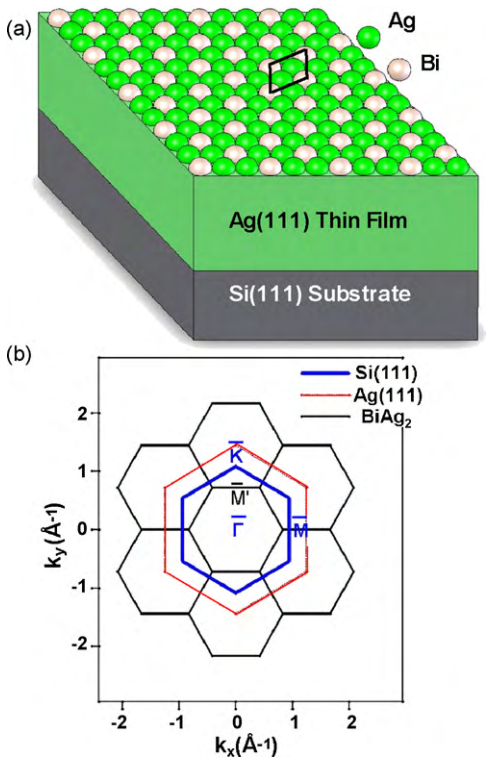


**Fig. 4.** (a) A schematic illustration of the $BiAg_2$–Ag–Si(1 1 1) structure. (b) Surface Brillouin zones of the $BiAg_2$ surface alloy (black), the Ag buffer layer (red) and the Si(1 1 1) substrate (blue). Primed (unprimed) letters refer to the high-symmetry points of the reconstruction (substrate). (For interpretation of the references to color in this figure legend, the reader is referred to the web version of the article.)

cessive images of Fig. 2 and a rigid energy shift was introduced from Fig. 3a to Fig. 3f as discussed earlier. The unoccupied part of the image was fitted using the calculated dispersion by Bihlmayer et al. [12]. Even for the highest Na coverage, the $p_{xy}$ spin degeneracy point remains about 350 meV away from the Fermi level. Therefore, it is hard to attain the exotic $E_F < E_0$ regime [20] due to saturation and the structural disorder. Spin-resolved measurements would be necessary in order to verify that the induced disorder does not modify the spin structure [15].

Even with these limitations, Fig. 2 proves that it is possible to tailor the spin-polarized electronic structure near $E_F$ by alkali metal doping. A similar shift of the Bi-derived states was accomplished in the $Bi_xPb_{1-x}$/Ag(1 1 1) system but the surface states were shifted to lower $E_B$ and their parameters were continuously changing from those of $BiAg_2$ to the ones of $PbAg_2$ [14]. The present study, on the other hand, represents a rigid shift of the alloy-derived bands and reveals the interesting possibility of obtaining new information about the band dispersion in the former unoccupied region by simple electron doping.

### 3.2. $BiAg_2$–Ag–Si(1 1 1)

Tunability of the spin polarization vector of a $BiAg_2$ surface alloy can be also achieved by growing the trilayer system depicted in Fig. 4a. Instead of forming the $BiAg_2$ alloy on a clean Ag(1 1 1) single crystal, we used a silver buffer layer which is itself deposited on a clean Si(1 1 1) $7 \times 7$ substrate. The present approach reports on two different interesting aspects of the SO-induced splitting. On one hand, it combines the giant RB effect with a semiconducting substrate, as it has been recently achieved for similar Bi-based systems [21,22]. On the other hand it offers the possibility to tune the spin structure near $E_F$ by modifying the thickness of the Ag buffer layer.

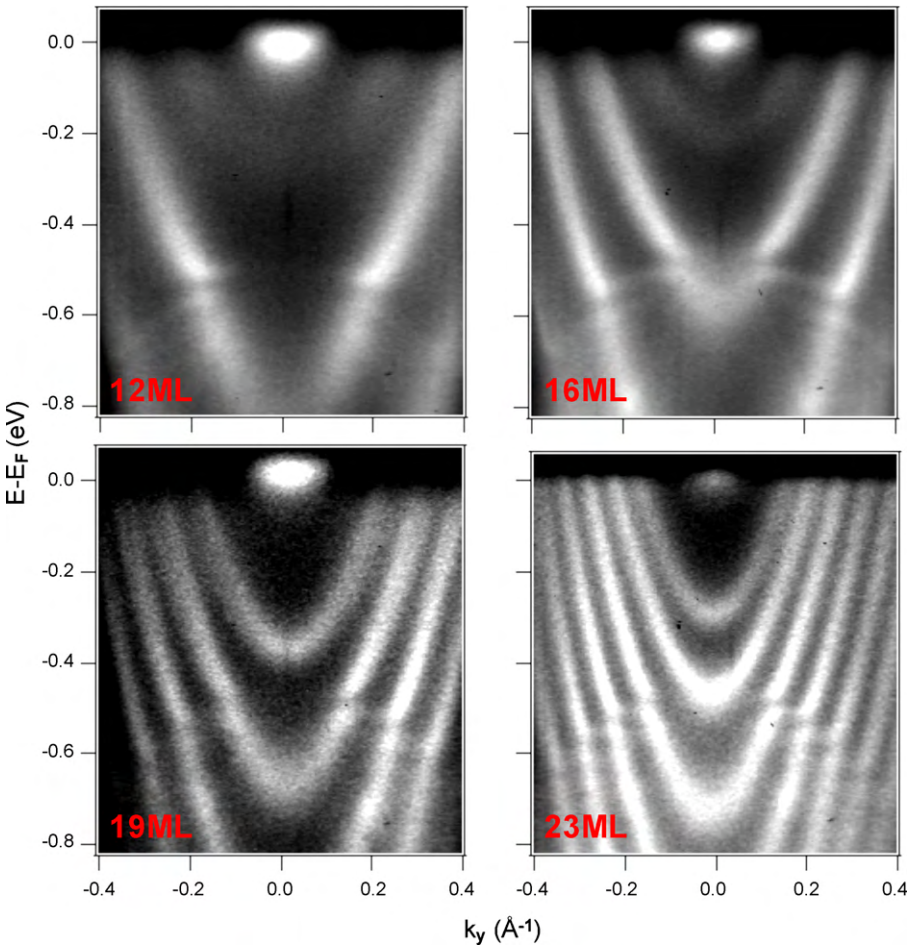


**Fig. 5.** ARPES intensity (70 K) around $\bar{\Gamma}$ for a thin Ag film grown on a Si(1 1 1) substrate. The quantum confinement of the bulk sp bands in the perpendicular direction results in QWS with parabolic dispersion. The number and energy position of the QWS depend on the thin film thickness.

The self-organization of Ag atoms deposited on a cold Si(1 1 1) $7 \times 7$ substrate yields a close-packed structure after a mild annealing. Ag/Si(1 1 1) is an incommensurate interface but atomically flat silver surfaces with a (1 1 1) termination plane grow if the deposited material exceeds the amount of 6 ML [23]. When the thickness of the Ag thin film is large (i.e. $d > 40$ ML), the latter behaves exactly as a Ag(1 1 1) single crystal. ARPES results on the clean film exhibit the well-studied Ag Shockley surface state. After the deposition of 1/3 ML Bi and the formation of the $BiAg_2$ alloy, the experimental data is identical to the surface electronic structure of the pure $BiAg_2$–Ag(1 1 1) system already described in the previous section (Fig. 2a).

An interesting situation arises for thinner Ag buffer layers, where $d$ is of the order of a few MLs. Before the deposition of Bi and the formation of the alloy, the Ag 5s states are confined within the Ag film by the potential barrier on the vacuum side and by the fundamental bandgap of Si on the substrate side. This confinement leads to quantized wave vectors along $z$ and to discrete energy levels in a "particle in a box" fashion. On the other hand, the electrons are nearly free in the $x$–$y$ plane and this yields a parabolic dispersion which is only perturbed when the energy approaches the maximum of the Si valence band [24]. The bulk continuum of the Ag 5s states is therefore replaced by these quantum-well states (QWS) as shown in Fig. 5. Their number and energy position are directly related to the thickness of the buffer layer and can be tuned at one's will.

When the $BiAg_2$ surface alloy is grown at the interface with a thin buffer layer, its surface electronic structure is significantly modified (Fig. 6) [25,26]. The spectral features are sharper than the thick-layer case because the alloy-derived states do not hybridize with the 5s bulk continuum but only at the intersections with the Ag QWS. As evidenced by the experimental results, hybridization with the confined states is strong enough to significantly alter the dispersion of the surface states. Hybridization gaps are clearly seen in the dispersion of the branches of both the inner ($sp_z$) and the outer ($p_{xy}$) bands. They form at the intersection of the spin-split alloy states with the nearly spin-degenerate Ag QWS. As a result, large and opposite values of the spin polarization are achieved at opposite sides of each mini-gap [25]. Interestingly, the number, energy and width of the hybridization gaps can be modified by varying the value of an external parameter (i.e. the buffer layer thickness).

In order to model the interaction between the QWS and the SS, and explain our experimental results, we extended the Hamiltonian matrix of the previous section. In Fig. 7 we considered the effect of two spin-degenerate QWS. The basis vectors are now $|sp_z\uparrow\rangle$, $|sp_z\downarrow\rangle$, $|p_{xy}\downarrow\rangle$, $|p_{xy}\uparrow\rangle$, $|sp_z\uparrow\rangle$, $|QW_1\uparrow\rangle$, $|QW_1\downarrow\rangle$, $|QW_2\uparrow\rangle$, $|QW_2\downarrow\rangle$, and our Hamiltonian matrix can be written as:

$$\begin{pmatrix} H_{SO}(sp_z) & V_{SS} & V_{(sp_z-QW_1)} & V_{(sp_z-QW_2)} \\ V_{SS}^* & H_{SO}(p_{xy}) & V_{(p_{xy}-QW_1)} & V_{(p_{xy}-QW_2)} \\ V_{(sp_z-QW_1)}^* & V_{(p_{xy}-QW_1)}^* & H_0(QW_1) & 0 \\ V_{(sp_z-QW_2)}^* & V_{(p_{xy}-QW_2)}^* & 0 & H_0(QW_2) \end{pmatrix}$$

This Hamiltonian matrix consists of sixteen $2 \times 2$ building blocks, each one referring to states of two different spins. $H_0$ denotes the free-electron-like dispersion of the QWS and the V building blocks

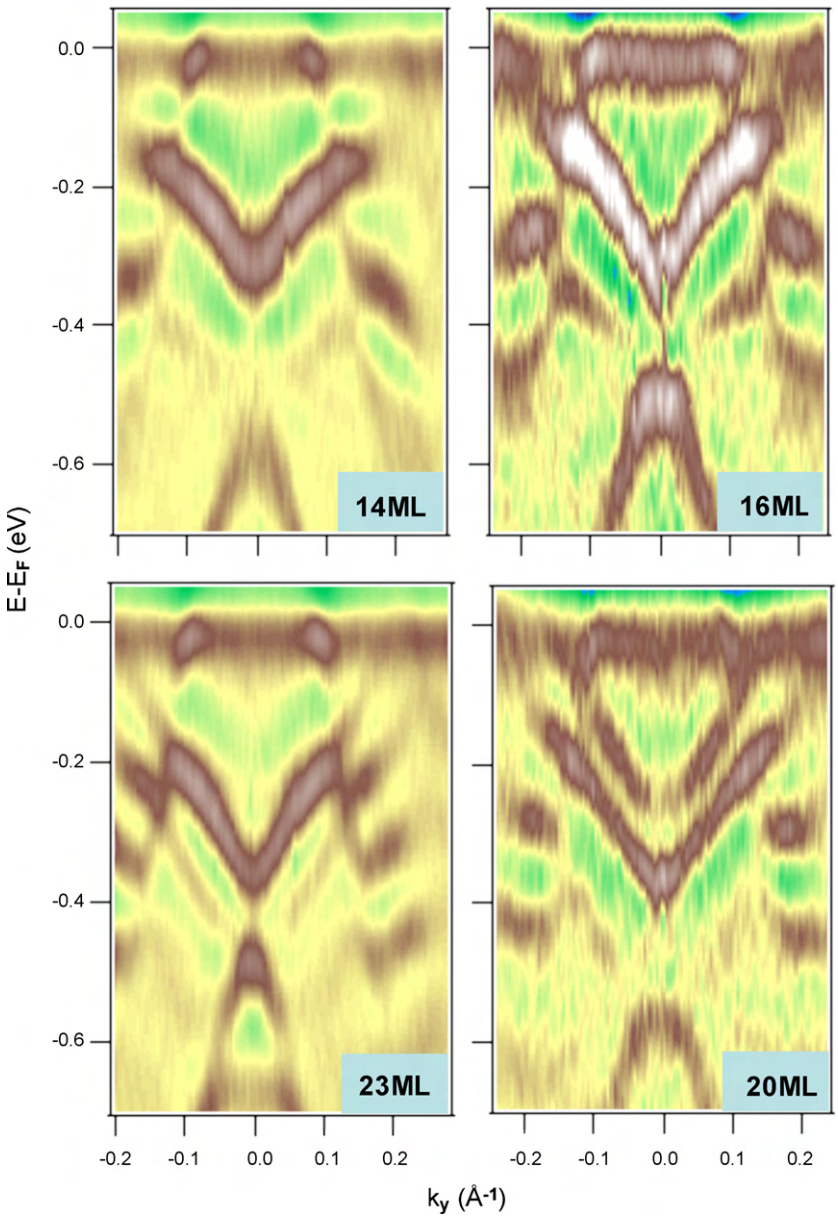


**Fig. 6.** ARPES intensity (70 K) around $\bar{\Gamma}$ for a $BiAg_2$–Ag–Si(1 1 1) surface alloy grown on a buffer layer of four different thicknesses. Intensity modulations along the dispersion of both the $p_{xy}$ and the $sp_z$ spin-split branches reveal the presence of hybridization gaps. A weak signature of the Ag QWS is also visible. The gap parameters can be tuned by varying the buffer layer thickness. The 2nd derivative of the photoemission intensity is shown in order to enhance the experimental data.

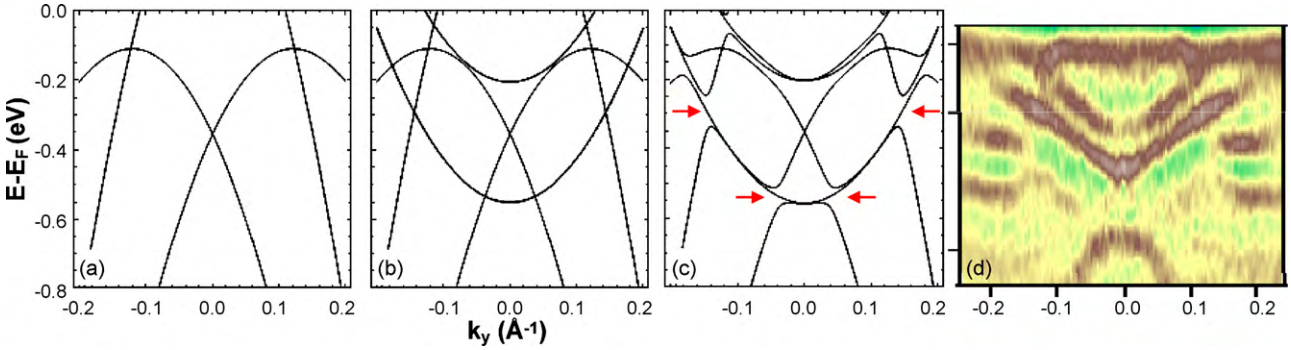


**Fig. 7.** Surface state and QWS dispersion around $\bar{\Gamma}$ for a $BiAg_2$–Ag–Si(1 1 1) surface alloy according to a simple hybridization model. (a) Only the calculated surface states dispersion is presented. (b) Two parabolic QWS are included but their interaction with the surface states is neglected. The QWS parameters mimic the 20 ML case. (c) As in (b) but the QWS interact with surface states of the same spin. The predicted discontinuities in the dispersion of the spin-split branches are pointed out by horizontal arrows. The weak hybridization of surface states has been neglected. (d) Experimental surface state and QWS dispersion for a $BiAg_2$ surface alloy grown on a 20 ML buffer layer. The energy positions of the gaps correspond well to the model's predictions. The 2nd derivative of the photoemission intensity is shown in order to enhance the experimental data.

refer to the hybridization between the two SS or between one QWS and one SS. The zero's point out that there is no hybridization between the two QWS. The hybridization between the QWS and the two spin-split pairs is parametrized by the corresponding potentials. These potentials are set to zero for states of opposite spins [27]. In general, the hybridization parameters may depend on the quantum number (n) of the QWS. This is because the SS do not have a fixed $sp_z$ or $p_{xy}$ character, but these relative components depend on their *k*-distance from the center of the SBZ [12]. Therefore, QWS of different n may interact with SS of a slightly modified character. The QWS have been considered as spin-degenerate before their interaction with the spin-split SS because their negligible splitting is beyond our experimental resolution and has not been observed by other high-resolution studies (e.g. [24]). On the other hand, a very small spin-splitting of Pb QWS has been recently found by Dil et al. for ultrathin Pb films on Si(1 1 1) [28]. Nevertheless, Ag, due to its smaller SO coupling constant, is expected to exhibit an even weaker splitting which can be safely approximated by zero. This is confirmed by our simple simulation (data not shown). An equivalent approach has been performed by He et al. [26] but without considering the effect of the in-plane potential into the shape of the momentum distributions.

Fig. 7c summarizes our qualitative results. In agreement with the experiment, the model predicts modulations in the dispersion of the spin-split branches, which are pointed out by horizontal arrows. However, these modulations do not correspond to real electronic gaps because our model assumes that the SS are always 100% spin polarized. The spin-polarized SS interact only with the QWS component of the same spin, leaving the opposite spin component unchanged. Nevertheless, inside such mini-gaps, the photoemission intensity should be dramatically decreased due to the weak signature of the QWS and the deviation from 100% spin-polarized SS. For reasons of clarity, Fig. 7b considers the same QWS and SS but without any interaction between them. The energy positions of the QWS mimic the 20 ML case (see Fig. 7d). Interestingly, as evidenced in Fig. 7c, hybridization effects can lift the spin degeneracy of the QWS resulting into a small but finite splitting. This is in agreement with the predictions of recent relativistic calculations [25].

The experimental data and our simple model agree that the interaction between confined QWS and SS with giant RB splitting results in the formation of spin-dependent gaps whose parameters depend on the buffer layer thickness. This opens up the interesting possibility to custom tailor the electronic structure and spin structure near $E_F$, thereby controlling the spin-polarized conduction.

## 4. Conclusions

We reported on two different experimental ways for tuning the Rashba-split states on the $BiAg_2$ surface alloy. Our approaches provide a means to modify the spin polarization near the Fermi level by tuning external parameters. Thereby, this opens the possibility to alter the spin transport in a future spintronic device. To this end, we have successfully transferred the concept of giant RB splitting on a semiconducting substrate. A simple hybridization model reproduces the main features of the experimental results.

## Acknowledgements

E.F. acknowledges the Alexander S. Onassis Public Benefit Foundation for the award of a scholarship. This research was supported by the Swiss NSF and the NCCR MaNEP.

## Appendix A.

The visualization of the hybridization model was performed with the software Mathematica 7.0 by Wolfram Research. The model's parameters are purely phenomenological and are summarized in the following tables.

See Tables A1–A4.

**Table A1**
Effective mass value as entered in the $H_{SO}$ Hamiltonian [18].

| Effective mass (as entered in the $H_{SO}$ Hamiltonian) | |
|---|---|
| $sp_z$ | −0.029 |
| $p_{xy}$ | −0.025 |
| $QW_1$ | 0.04 |
| $QW_2$ | 0.04 |

**Table A2**
Anisotropy parameter value as entered in the $H_{SO}$ Hamiltonian [18].

| Anisotropy parameter (in eV Å$^3$) | |
|---|---|
| $sp_z$ | 23 |
| $p_{xy}$ | 21 |
| $QW_1$ | 0 |
| $QW_2$ | 0 |

**Table A3**
Spin–orbit parameter value as entered in the $H_{SO}$ Hamiltonian [18].

| SO parameter (in eV Å) | |
|---|---|
| $sp_z$ | 4.1 |
| $p_{xy}$ | 3.3 |
| $QW_1$ | 0 |
| $QW_2$ | 0 |

**Table A4**
Hybridization potential between different electronic states.

| Hybridization potential (1st Fourier coefficient in eV) | |
|---|---|
| $sp_z$–$p_{xy}$ | −0.02 |
| QW–$sp_z$ | −0.02 |
| QW–$p_{xy}$ | −0.05 |

## References

[1] Y.A. Bychkov, E.I. Rashba, JETP Lett. 39 (1984) 78.
[2] G. Dresselhaus, Phys. Rev. 100 (1955) 580.
[3] S.A. LaShell, B.A. McDougall, E. Jensen, Phys. Rev. Lett. 77 (1996) 3419.
[4] L. Petersen, P. Hedegård, Surf. Sci. 459 (2000) 49.
[5] D. Malterre, B. Kierren, Y. Fagot-Revurat, S. Pons, A. Tejeda, C. Didiot, H. Cercellier, A. Bendounan, New J. Phys. 9 (2007) 391.
[6] F. Reinert, J. Phys.: Condens. Matter 15 (2003) S693.
[7] Y.M. Koroteev, G. Bihlmayer, J.E. Gayone, E.V. Chulkov, S. Blügel, P.M. Echenique, P. Hofmann, Phys. Rev. Lett. 93 (2004) 046403.
[8] E. Rotenberg, J. Chung, S. Kevan, Phys. Rev. Lett. 82 (1999) 4066.
[9] M. Hochstrasser, J. Tobin, E. Rotenberg, S. Kevan, Phys. Rev. Lett. 89 (2002) 216802.
[10] C.R. Ast, J. Henk, A. Ernst, L. Moreschini, M.C. Falub, D. Pacilé, P. Bruno, K. Kern, M. Grioni, Phys. Rev. Lett. 98 (2007) 186807.
[11] J. Premper, M. Trautmann, J. Henk, P. Bruno, Phys. Rev. B 76 (2007) 073310.
[12] G. Bihlmayer, S. Blügel, E.V. Chulkov, Phys. Rev. B 75 (2007) 195414.
[13] S. Datta, B. Das, Appl. Phys. Lett. 56 (1990) 665.
[14] C.R. Ast, D. Pacilé, L. Moreschini, M.C. Falub, M. Papagno, K. Kern, M. Grioni, Phys. Rev. B 77 (2008) 081407.
[15] F. Meier, V. Petrov, S. Guerrero, C. Mudry, L. Patthey, J. Osterwalder, J.H. Dil, Phys. Rev. B 79 (2009) 241408.
[16] H. Bentmann, F. Forster, G. Bihlmayer, E.V. Chulkov, L. Moreschini, M. Grioni, F. Reinert, EPL 87 (2009) 37003.
[17] F. Meier, H. Dil, J. Lobo-Checa, L. Patthey, J. Osterwalder, Phys. Rev. B 77 (2008) 165431.
[18] H. Mirhosseini, J. Henk, A. Ernst, S. Ostanin, C.-T. Chiang, P. Yu, A. Winkelmann, J. Kirschner, Phys. Rev. B 79 (2009) 245428.
[19] L. Fu, Phys. Rev. Lett. 103 (2009) 266801.
[20] E. Cappelluti, C. Grimaldi, F. Marsiglio, Phys. Rev. Lett. 98 (2007) 167002.
[21] I. Gierz, t. Suzuki, E. Frantzeskakis, S. Pons, S. Ostanin, A. Ernst, J. Henk, M. Grioni, K. Kern, C.R. Ast, Phys. Rev. Lett. 103 (2009) 046803.

[22] K. Sakamoto, H. Kakuta, K. Sugawara, K. Miyamoto, A. Kimura, T. Kuzumaki, N. Ueno, E. Annese, J. Fujii, A. Kodama, T. Shishidou, H. Namatame, M. Taniguchi, T. Sato, T. Takahashi, T. Oguchi, Phys. Rev. Lett. 103 (2009) 156801.
[23] L. Huang, S.J. Chey, J.H. Weaver, Surf. Sci. 416 (1998) L1101.
[24] N. Speer, S. Tan, T.C. Chiang, Science 314 (2006) 804.
[25] E. Frantzeskakis, S. Pons, H. Mirhosseini, J. Henk, C.R. Ast, M. Grioni, Phys. Rev. Lett. 101 (2008) 196805.
[26] K. He, T. Hirahara, T. Okuda, S. Hasegawa, A. Kazizaki, I. Matsuda, Phys. Rev. Lett. 101 (2008) 107604.
[27] C. Didiot, Y. Fagot-Revurat, S. Pons, B. Kierren, C. Chatelain, D. Malterre, Phys. Rev. B 74 (2006) 081404.
[28] J.H. Dil, F. Meier, J. Lobo-Checa, L. Patthey, G. Bihlmayer, J. Osterwalder, Phys. Rev. Lett. 101 (2008) 2466802.